

**Cite this article as:** Li Yuli, Li Hao, Chen Qiuyu, et al. Hot Deformation Behavior and Processing Map of Zr-Sn-Nb-Fe-Cr Alloy[J]. Rare Metal Materials and Engineering, 2025, 54(07): 1671-1677. DOI: <https://doi.org/10.12442/j.issn.1002-185X.20240519>.

ARTICLE

# Hot Deformation Behavior and Processing Map of Zr-Sn-Nb-Fe-Cr Alloy

Li Yuli, Li Hao, Chen Qiuyu, Zhou Xuan, Ma Tianyang, Sun Taotao

*Xi'an Western Energy Material Technologies Co., Ltd, Xi'an 710016, China*

**Abstract:** The hot deformation characteristics of induction quenched Zr-Sn-Nb-Fe-Cr alloy forged rod in the temperature range of 600–900 °C and strain rate range of 0.001–1 s<sup>-1</sup> were studied by Gleeble3800 uniaxial hot compression experiment. The results show that the flow stress decreases with the decrease in strain rate and the increase in deformation temperature in the true stress-true strain curve of Zr-Sn-Nb-Fe-Cr alloy forged rod. Moreover, the hot deformation characteristics of the material can be described by the hyperbolic sine constitutive equation. Under the experimental conditions, the average thermal activation energy (Q) of the alloy was 412.9105 kJ/mol. The microstructure analysis of the processing map and the sample after hot compression shows that the optimum hot working parameters of the alloy are 795–900 °C, 0.001–0.0068 s<sup>-1</sup>, at the deformation temperature of 600–900 °C, and the strain rate of 0.001–1 s<sup>-1</sup>.

**Key words:** zirconium alloy; constitutive equation; hot deformation; processing map

## 1 Introduction

In addition to neutron radiation, high fatigue strength, and excellent thermal conductivity, zirconium and its alloys also have excellent mechanical properties and corrosion resistance, which are used as fuel cladding and structural component materials in nuclear power reactors<sup>[1–4]</sup>. However, modern nuclear reactors have been developed in the direction of higher thermal efficiency, so traditional zirconium alloys and binary Zr-Nb alloys are no longer suitable for use under enhanced burn-up conditions, which leads to the development of new zirconium alloys with enhanced performance in recent years<sup>[5–9]</sup>. These include ZIRLO (Zr-1.0Nb-1.0Sn-0.1Fe)<sup>[10]</sup>, M5 (Zr-1Nb-0.125O)<sup>[5]</sup>, E635 (Zr-1.0Nb-1.0Sn-0.4Fe)<sup>[11]</sup>, HANA-4 (Zr-1.5Nb-0.4Sn-0.2Fe-0.1Cr)<sup>[12]</sup>, and N18 (Zr-1.0Nb-0.3Sn-0.3Fe)<sup>[13]</sup>. However, the current research mainly focused on the properties of corrosion<sup>[13–15]</sup>, creep, and irradiation growth<sup>[16–17]</sup> of these new zirconium alloys, and the hot processing properties of these zirconium alloys were less studied.

Nuclear grade zirconium alloys are often used as cladding materials for nuclear reactors, so their manufacturing processes involve considerable machining, such as multi-fire

forging hot working after the melting stage, heat treatment, hot extrusion, and later cold working steps to achieve the required strength, suitable microstructure, and dimensional tolerance<sup>[18–19]</sup>. Among these steps, hot working in the form of forging and extrusion is very important, which is also responsible for providing chemical uniformity in addition to breaking the cast microstructure and shaping the ingot<sup>[20]</sup>. The hot deformation behavior of metal material reflects the law of microstructure evolution during the process of hot deformation<sup>[21–23]</sup>. The stress, deformation temperature, and strain rate are the main factors affecting the microstructure and properties of zirconium alloy<sup>[24–26]</sup>.

In this study, the hot deformation behavior of the induction quenched Zr-Sn-Nb-Fe-Cr alloy forged rod at different deformation temperatures and strain rates was studied. The relationship between flow stress and strain, deformation temperature and strain rate were summarized to reveal the hot deformation behavior of the alloy. And the constitutive equation describing the hot deformation of the alloy was established. Based on the dynamic materials model (DMM), the processing map of the alloy was established, which provided the theoretical basis for the optimization of the

Received date: August 14, 2024

Foundation item: CNNC Youth Talent Program (CNNC-SFTYS-202201)

Corresponding author: Li Hao, Ph.D., Xi'an Western Energy Material Technologies Co., Ltd, Xi'an 710016, P. R. China, E-mail: [lihao\\_wem@163.com](mailto:lihao_wem@163.com)

Copyright © 2025, Northwest Institute for Nonferrous Metal Research. Published by Science Press. All rights reserved.

hot deformation process parameter in the actual production of the alloy.

## 2 Experiment

The Zr-Sn-Nb-Fe-Cr alloy ingot with uniform composition was obtained by vacuum consumable melting (triple melting), and the chemical composition is shown in Table 1. The total tin (T. Sn), total niobium (T. Nb), total iron (T. Fe), and total chromium (T. Cr) contents in the alloy ingot were analyzed using an inductively coupled plasma (ICP), and the gas elements were analyzed using a LECO oxygen & nitrogen analyzer. After melting, the ingot was machined into a cylinder with a diameter of 650 mm. The first-time forging was conducted at 1070 °C, and the ingot was forged into a round rod with a diameter of 300 mm. The second-time forging was conducted at 980 °C, and the alloy round rod with a diameter of 300 mm was forged into the extrusion billet with a diameter of 252 mm. The final temperature of all the forging processes must be  $\geq 600$  °C. The quenching process of the alloy was induction quenching with the holding temperature of 1070 °C and the holding time of 5 min.

Samples with the size of  $\Phi 10$  mm $\times$ 15 mm were processed from the induction quenched Zr-Sn-Nb-Fe-Cr alloy forged rod, and the hot compression test was conducted on the Gleeble3800 thermal simulation machine. The deformation temperatures were set at 600, 675, 750, 825, and 900 °C. The strain rates were set at 0.001, 0.01, 0.1, and 1 s<sup>-1</sup>. The maximum deformation of test samples was 60%. Three parallel experiments were conducted at each temperature and each strain rate, and the most stable experimental data were selected. The machine automatically collected data during the experiment, and then Origin and Matlab software were used to analyze the data. Before the hot compression deformation, all samples were rapidly heated to the pre-set deformation temperature at a heating rate of 10 °C/s, and kept for 2 min to ensure the uniform distribution of sample temperature. After the deformation, the samples were quickly taken out for water cooling and the high-temperature microstructures after the high temperature deformation were obtained. After the Gleeble test, the samples after hot compression and water-cooled quenching were polished and etched with a corrosive agent of 10 mL HF+45 mL HNO<sub>3</sub>+45 mL H<sub>2</sub>O, and the microstructure was characterized by scanning electron microscope (SEM). As shown in Fig.1, the microstructure of Zr-Sn-Nb-Fe-Cr alloy forged rod after induction quenching was mainly composed of basketweave-like Widmanstätten structures, which was formed from the grain boundary of the original  $\beta$  grain.

**Table 1 Chemical composition of Zr-Sn-Nb-Fe-Cr alloy ingot (wt%)**

Sn	Nb	Fe	Cr	H	O	N
0.98	0.30	0.36	0.64	0.0003	0.1028	0.0028

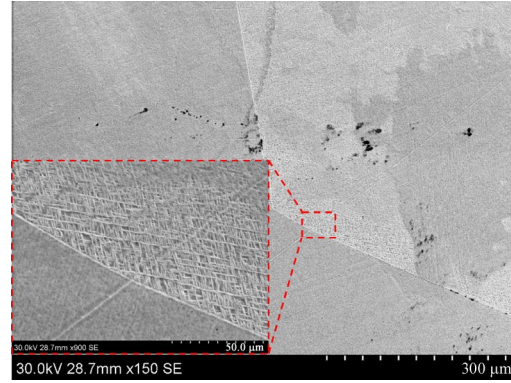


Fig.1 Microstructures of Zr-Sn-Nb-Fe-Cr forged rod after induction quenching

## 3 Results and Discussion

### 3.1 True stress-true strain curve

Fig.2 shows the true stress-true strain curves of induction quenched Zr-Sn-Nb-Fe-Cr alloy forged rod under different deformation conditions. The flow stress of the alloy increases rapidly at the initial stage of deformation, which should be attributed to the increase in dislocation density. These accumulated dislocations can significantly hinder further deformation, resulting in higher strength of the alloy<sup>[27]</sup>. Both temperature and strain rate have obvious effects on the flow stress of the alloy. Under the condition of constant strain rate, the flow stress of Zr-Sn-Nb-Fe-Cr alloy increases with the decrease in deformation temperature. This is due to the fact that higher temperatures make slip and dynamic recrystallization more likely to occur<sup>[28]</sup>. At the same time, the resistance of the secondary phase particles to deformation decreases<sup>[29]</sup>, which also helps to reduce the flow stress. At a fixed temperature, the flow stress of the alloy increases with the increase in strain rate. This phenomenon is because the alloy produced more dislocations per unit time at higher strain rates.

It is worth noting that when the temperature is 900 °C, the peak flow stress of the alloy is maintained at a certain level under all the strain rates. The hardening effect caused by dislocation generation and accumulation is offset by the softening effect caused by dynamic recrystallization in the alloy, and the dynamic balance is reached. When the strain rate is 1 s<sup>-1</sup>, the true stress-true strain curve presents a small wave shape, which is caused by the dominant role of dynamic recrystallization and work hardening. The increase in temperature supports the formation of dynamic recrystallization of Zr-Sn-Nb-Fe-Cr alloy, which is also promoted by the increase in dislocation density.

### 3.2 Hot deformation constitutive equation

From the point of view of mechanics and materials science, the accurate constitutive equation is very important to the metal hot working process. Strain rates, strain value, and deformation temperature are important parameters in the metal hot working process, and the constitutive equations

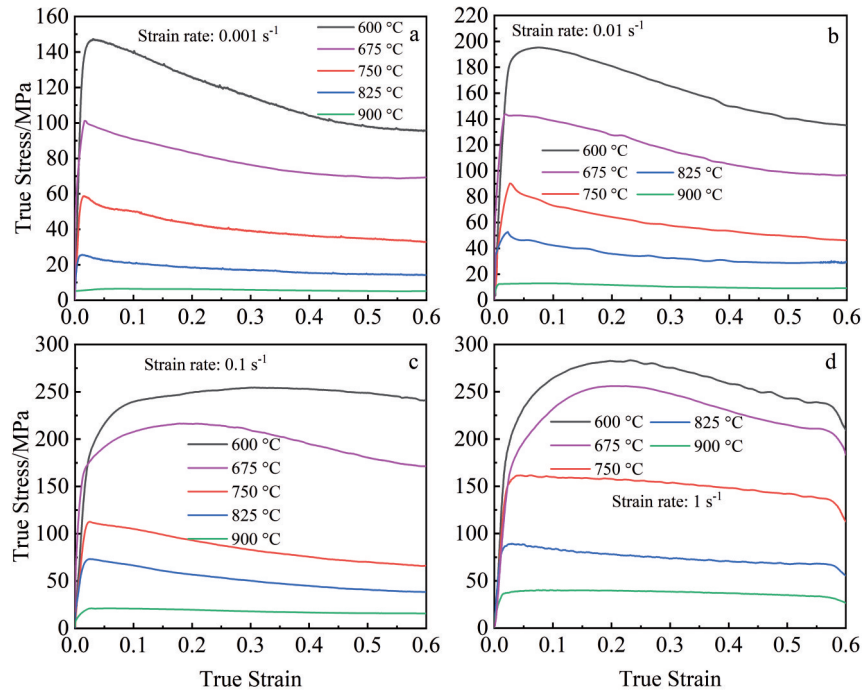


Fig.2 True stress-true strain curves of induction quenched Zr-Sn-Nb-Fe-Cr alloy forged rod under different strain rates: (a)  $0.001 \text{ s}^{-1}$ ; (b)  $0.01 \text{ s}^{-1}$ ; (c)  $0.1 \text{ s}^{-1}$ ; (d)  $1 \text{ s}^{-1}$

described the plastic flow characteristics of metals and alloys are also affected by these parameters. The flow stress serves not only as an important parameter for calculating the rolling or forging pressure during metal plastic deformation, but also as a diagnostic tool to reveal the microstructure change, property variations, and the law of plastic deformation in the process of hot deformation. The high temperature deformation of metal is a heat-activated process. When the strain ( $\epsilon$ ) was a certain value, the stress ( $\sigma$ ) of the material meets a certain functional relationship with the deformation temperature ( $T$ ) and strain rate ( $\dot{\epsilon}$ ). In this study, the hyperbolic sine model proposed by Sellars and Tegart<sup>[30]</sup> is used to describe the constitutive equation of the induction quenched Zr-Sn-Nb-Fe-Cr alloy forged rod, which can be expressed as Eq.(1):

$$\dot{\epsilon} = A \left\{ \left[ \sinh(\alpha\sigma) \right]^n \exp(-Q/RT) \right\} \quad (1)$$

At high temperature and low stress levels, the relationship between stress and strain rate is as follows:

$$\dot{\epsilon} = A_1 \sigma^{n_1} \exp(-Q/RT) \quad (2)$$

At low temperature and high stress levels, the relationship between stress and strain rate is as follows:

$$\dot{\epsilon} = A_2 \exp(\beta\sigma) \exp(-Q/RT) \quad (3)$$

where  $\dot{\epsilon}$  is the strain rate,  $\text{s}^{-1}$ ;  $\sigma$  is stress, MPa;  $Q$  is the activation energy of deformation heat, J/mol;  $R$  is the gas constant,  $8.314 \text{ J}/(\text{K}\cdot\text{mol})$ ;  $T$  is the absolute temperature, K;  $A$ ,  $\alpha$ ,  $n$ ,  $\beta$ ,  $A_1$ ,  $A_2$ ,  $n_1$  are material constants, and  $\alpha = \beta/n_1$ .

At a constant deformation temperature, take the logarithm on both sides of Eq. (3) and Eq. (2) and rearrange them to obtain Eq. (4) and Eq. (5), respectively, as follows:

$$\ln \dot{\epsilon} = \ln A_2 + \beta\sigma - \frac{Q}{RT} = \beta\sigma + \ln A'_2 \quad (4)$$

$$\ln \dot{\epsilon} = \ln A_1 + n_1 \ln \sigma - \frac{Q}{RT} = n_1 \ln \sigma + \ln A'_1 \quad (5)$$

Fig. 3 shows linear regression graphs for  $\ln \dot{\epsilon} - \ln \sigma$  and  $\ln \dot{\epsilon} - \sigma$  based on the obtained data after the peak flow stress value in

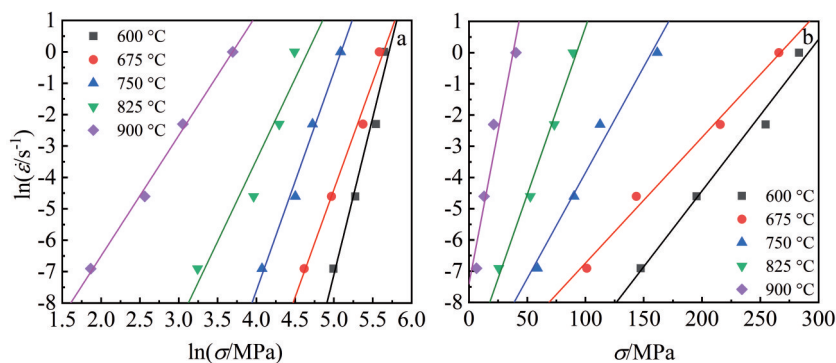


Fig.3 Linear relationship between stress and strain rate at different temperatures: (a)  $\ln \dot{\epsilon} - \ln \sigma$ ; (b)  $\ln \dot{\epsilon} - \sigma$

Fig. 2 substituted into Eq. (5) and Eq. (4). According to Eq.(4-5), the mean value of material constant  $\beta$  and  $n_1$  of the alloy is 0.1385 and 6.2614 when deformed at low temperature and high stress levels, respectively. Thus, it can be found that  $\alpha = \beta/n_1 = 0.0221$ .

When the deformation temperature is fixed, the logarithm on both sides of Eq. (1) can be obtained as follows:

$$\ln \dot{\epsilon} = \ln A + n \ln [\sinh(\alpha \sigma)] - Q/RT \quad (6)$$

The following Eq. (6) is arranged:

$$\ln [\sinh(\alpha \sigma)] = \frac{1}{n} \ln \dot{\epsilon} + \frac{1}{n} \left( \frac{Q}{RT} - \ln A \right) = \frac{1}{n} \ln \dot{\epsilon} + \ln A' \quad (7)$$

For a given strain rate, the partial derivative of  $\ln[\sinh(\alpha \sigma)]$  with respect to  $1/T$  is as follows:

$$Q = nR \left( \frac{d \{ \ln [\sinh(\alpha \sigma)] \}}{d(1/T)} \right) \quad (8)$$

The linear regression diagram of  $\ln \dot{\epsilon} - \ln[\sinh(\alpha \sigma)]$  is shown in Fig. 4a. The slope ( $n$ ) of  $\ln \dot{\epsilon} - \ln[\sinh(\alpha \sigma)]$  is obtained by fitting the line according to Eq. (6), and its value is 3.1558. The value of deformation activation energy  $Q$  is obtained from the slope ( $Q/nR$ ) of  $\ln[\sinh(\alpha \sigma)] - 1000/T$  fitted line, as shown in Fig. 4b. The mean value of hot deformation activation energy at different strain rates is 412.9105 kJ/mol calculated from Eq. (8), and the value of  $A$  at different temperatures and strain rates are calculated from Eq. (1). The average value is  $4.2905 \times 10^{18}$ .

The expression for the Zener-Hollomon ( $Z$ ) parameter is as follows:

$$Z = \dot{\epsilon} \exp \left( - \frac{Q}{RT} \right) = A [\sinh(\alpha \sigma)]^n \quad (9)$$

Taking the logarithm on both sides of the Eq. (9), get the following Eq. (10):

$$\ln Z = \ln A + n \ln [\sinh(\alpha \sigma)] \quad (10)$$

The relationship curve of  $\ln[\sinh(\alpha \sigma)] - \ln Z$  is drawn by least square linear regression, as shown in Fig.5, with small relative error and high precision. The results show that the model can be used to describe the high temperature deformation behavior of the induction quenched Zr-Sn-Nb-Fe-Cr alloy rod.

The values of all parameters are substituted into Eq. (1) and Eq. (3), and the obtained true strain-true stress relationship equation can be expressed by the following function:

$$\sigma = \frac{1}{\alpha} \ln \left\{ \left( \frac{Z}{A} \right)^{\frac{1}{n}} + \left[ \left( \frac{Z}{A} \right)^{\frac{2}{n}} + 1 \right]^{\frac{1}{2}} \right\} \quad (11)$$

In order to verify the accuracy of the obtained constitutive equation, the values of peak stress under different deformation conditions are calculated by substituting different temperatures and strain rates into Eq. (11), and the results are compared with the test values, as shown in Fig.6. The average error between the calculated value and the experimental value is less than 5%, indicating that the hyperbolic sine constitutive equation can be used to describe the deformation behavior of the induction quenched Zr-Sn-Nb-Fe-Cr alloy rod, and can provide guidance for the equation of the subsequent hot forming process.

### 3.3 Processing map

Based on DDM model<sup>[31-32]</sup>, the power dissipation coefficient  $\eta$  can be expressed by Eq.(12):

$$\eta = \frac{J}{J_{\max}} = m/(m+1) \quad (12)$$

where  $J$  is the energy dissipated due to microstructural evolution;  $J_{\max}$  denotes the ideal linear dissipative state with  $J$  reaching its maximum value;  $m$  is the strain rate sensitivity index, which can be expressed by Eq. (13):

$$m = \frac{\partial(\lg \sigma)}{\partial(\lg \dot{\epsilon})} = b + 2c \lg \dot{\epsilon} + 3d(\lg \dot{\epsilon})^2 \quad (13)$$

where  $b$ ,  $c$ , and  $d$  are material parameters. The instability diagram is based on the irreversible thermodynamics, and  $\zeta(\dot{\epsilon})$  is used to represent the continuous instability criterion, which is expressed by Eq. (14):

$$\zeta(\dot{\epsilon}) = \ln 10(m+1) \frac{2c + 6d(\lg \dot{\epsilon})}{m} + m \quad (14)$$

Matlab was used to process the peak stress data of induction quenched Zr-Sn-Nb-Fe-Cr alloy forged rod from hot compression test, draw the efficiency map of power dissipation and instability map of the material, and combine the two to form the processing map of the material, the results are shown in Fig. 7. Fig. 7a is the three-dimensional (3D) efficiency map of the power dissipation of the alloy under corresponding deformation conditions. The bottom is a two-dimensional graph formed by projection, and the contours in

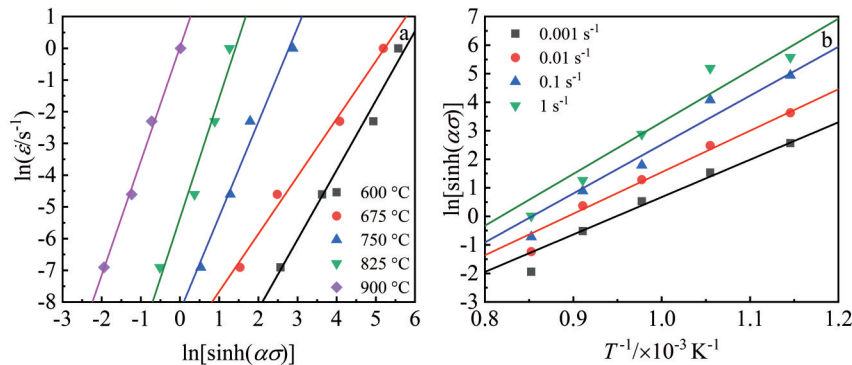


Fig.4 Linear relationship of  $\ln \dot{\epsilon} - \ln[\sinh(\alpha \sigma)]$  (a) and  $\ln[\sinh(\alpha \sigma)] - 1/T$  (b)

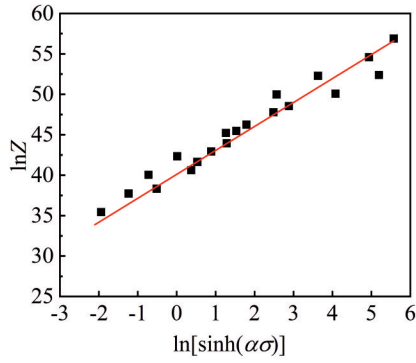


Fig.5 Relationship curve between  $\ln[\sinh(\alpha\sigma)]$  and  $\ln Z$

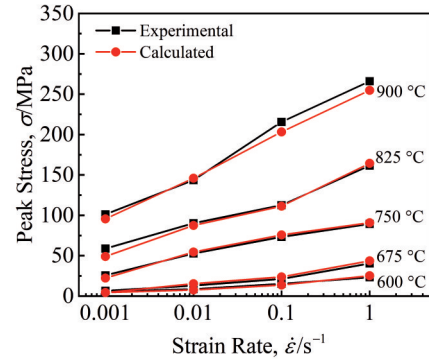


Fig.6 Experimental and calculated values of peak stress at different temperatures and strain rates

Fig. 7a represent the energy dissipation efficiency ( $\eta$ , %). Fig.7b is 3D instability map of the material. The region where  $\zeta(\dot{\epsilon})$  is less than zero is marked in blue, and the processing map of the material under study can be synthesized by superposing Fig.7a and Fig.7b, as shown in Fig.7c.

As can be seen from Fig.7b–7c, the safe processing regions of the alloy are relatively narrow, and the flow instability regions are more likely to occur at a high strain rate ( $\dot{\epsilon} \geq 0.1 \text{ s}^{-1}$ ) and temperature range of 600–680 °C. The alloy undergoes rapid deformation with insufficient coordination of deformation degree at high strain rates, resulting in inadequate time for the matrix to counteract the hardening effect caused by dislocation diffusion. Therefore, the zirconium alloy used in

this study is suitable for processing at high temperatures and low strain rates.

Fig. 8 shows the microstructure of the alloy after hot compression at different deformation temperatures and strain rate  $\dot{\epsilon} = 0.001 \text{ s}^{-1}$ . In the temperature range of 600–900 °C, the original grain size has a significant difference, indicating that the dynamic recrystallization tendency is different.

During the hot compression deformation in the temperature range of 600–750 °C, the original grain is elongated along the deformation direction. And due to the rapid water-cooling after deformation, a large number of basketweave-like Widmanstätten structures are generated inside the original grain,

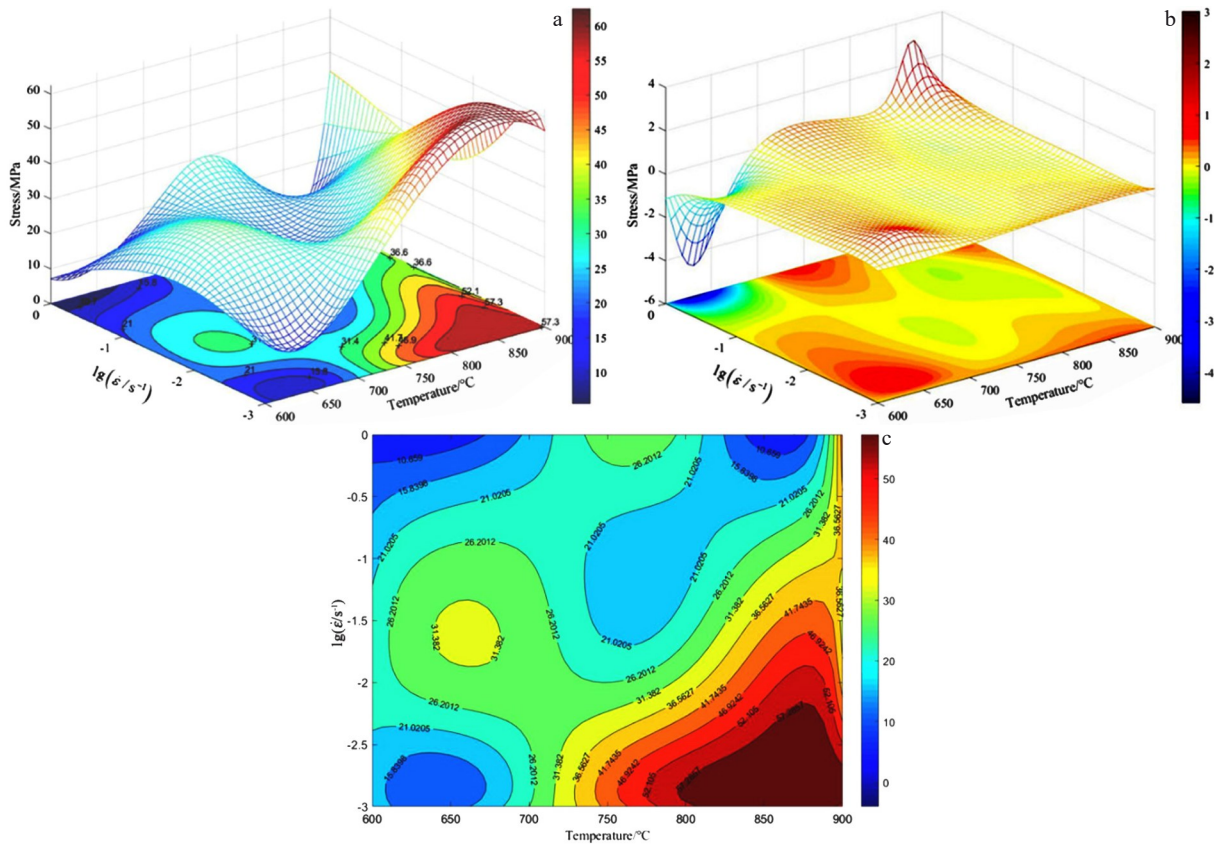


Fig.7 3D efficiency map of power dissipation (a), 3D instability map (b), and processing map (c) of induction quenched Zr-Sn-Nb-Fe-Cr alloy forged rod

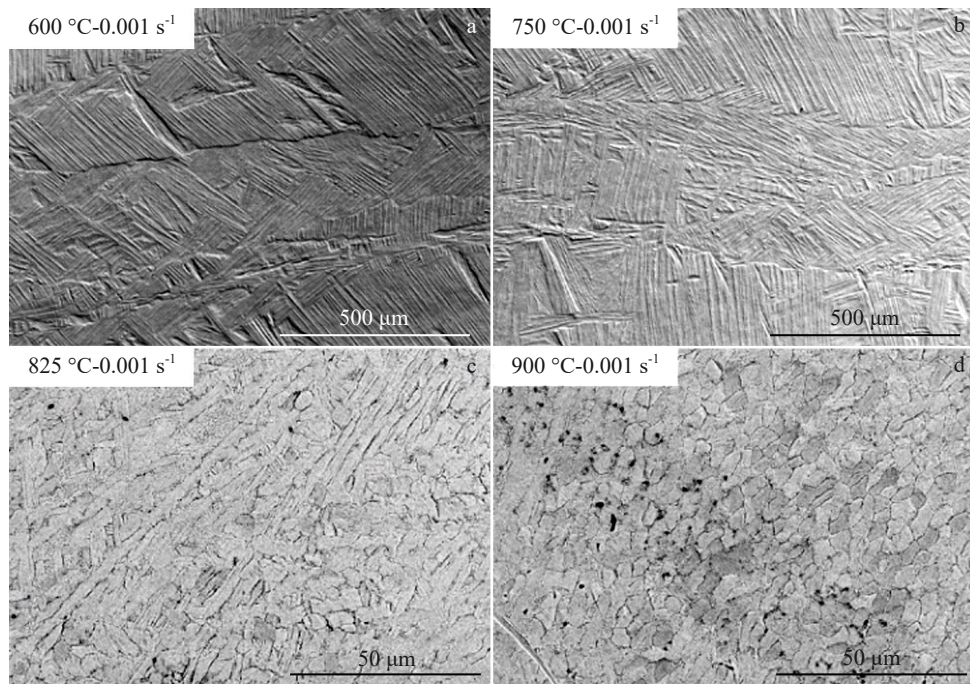


Fig.8 Microstructures of Zr-Sn-Nb-Fe-Cr alloy at different temperatures with strain rate of  $0.001 \text{ s}^{-1}$ : (a)  $600 \text{ }^{\circ}\text{C}$ ; (b)  $750 \text{ }^{\circ}\text{C}$ ; (c)  $825 \text{ }^{\circ}\text{C}$ ; (d)  $900 \text{ }^{\circ}\text{C}$

so it can be judged that the material has no recrystallization structure in the temperature range of  $600\text{--}750 \text{ }^{\circ}\text{C}$ .

When deformed at  $825 \text{ }^{\circ}\text{C}$ , the microstructure is in a mix-crystal state, the coarse crystals are the part without dynamic recrystallization, and the fine crystals occupy the majority, indicating that the dynamic recrystallization process is still not completed. With the increase in deformation temperature, the solid solubility of alloying elements increases, the secondary phase near the grain boundary decreases, and the effect of hindering dynamic recrystallization gradually weakens, resulting in dynamic recrystallization of deformed grains. At  $900 \text{ }^{\circ}\text{C}$ , complete dynamic recrystallization occurs and the dynamic recrystallization grains grow, indicating that the higher the deformation temperature at the same strain rates, the easier it is for grains formed by the dynamic recrystallization to grow, which is very consistent with the prediction of the processing map in Fig.7c.

#### 4 Conclusions

1) The analysis of the true stress-true strain curve of the induction quenched Zr-Sn-Nb-Fe-Cr alloy forged rod shows that the flow stress of the alloy decreases with the decrease in strain rates and the increase in deformation temperatures.

2) The hyperbolic sine constitutive equation can be used to describe the deformation behavior of the induction quenched Zr-Sn-Nb-Fe-Cr alloy forged rod, and the average thermal activation energy is obtained of  $Q=412.9105 \text{ kJ/mol}$ .

3) The processing map of the induction quenched Zr-Sn-Nb-Fe-Cr alloy forged rod and the microstructure analysis after hot compression showed that DMM theory is reliable and can be used as a useful tool to optimize the hot working parameters of the material. The optimum parameters of hot

working for the alloy in the range of  $600\text{--}900 \text{ }^{\circ}\text{C}$  are  $795\text{--}900 \text{ }^{\circ}\text{C}$  and  $0.001\text{--}0.0068 \text{ s}^{-1}$ .

#### References

- Gostariani R, Asadabad A M. *Journal of Materials Engineering and Performance*[J], 2023, 32: 2151
- Chen J, Shi H L, Lin G Y et al. *International Journal of Refractory Metals and Hard Materials*[J], 2024, 120: 106603
- Diniasi D, Golgovici F, Marin A H et al. *Materials*[J], 2021, 14(16): 4586
- Deng S Y, Song H W, Liu H et al. *International Journal of Solids and Structures*[J], 2021, 213: 63
- Saini S, Gayathri N, Sharma S K et al. *Journal of Nuclear Materials*[J], 2020, 528: 151894
- Liu J J, Wan K L, Lu S Q et al. *Journal of Nuclear Materials*[J], 2020, 531: 151993
- Saxena K K, Sonkar S, Pancholi V et al. *Journal of Alloys and Compounds*[J], 2016, 662: 94
- Saxena K K, Yadav S D, Sonkar S et al. *Procedia Materials Science*[J], 2014, 6: 278
- Coleman C E, Grigoriev V, Inozemtsev V et al. *Zirconium in the Nuclear Industry: 16th International Symposium*[C], West Conshohocken: ASTM International, 2012: 544
- Pu J, Zhang C H, Zhu W G et al. *Materials Characterization*[J], 2024, 212: 113932
- Nikulina A V, Markelov V, Peregud M M et al. *Zirconium in the Nuclear Industry: 11th International Symposium*[C], West Conshohocken: ASTM International, 1996: 785
- Jung Y I, Lee M H, Kim H G et al. *Journal of Alloys and*

- Compounds[J], 2009, 479(1-2): 423
- 13 Zhao Wenjin, Miao Zhi, Jiang Hongman. *Journal of Chinese Society for Corrosion and Protection*[J], 2009, 22(2): 124 (in Chinese)
- 14 Park J Y, Choi B K, Yoo S J et al. *Journal of Nuclear Materials*[J], 2006, 359(1-2): 59
- 15 Kim H G, Jeong Y H, Kim T H. *Journal of Nuclear Materials*[J], 2004, 326(2-3): 125
- 16 Jeong Y H, Kim H G, Kim D J et al. *Journal of Nuclear Materials*[J], 2003, 323(1): 72
- 17 Zhou B X, Yao M Y, LI Z K et al. *Journal of Materials Science & Technology*[J], 2012, 28(7): 606
- 18 Kapoor R, Chakravarty J K. *Journal of Nuclear Materials*[J], 2002, 306(2-3): 126
- 19 Lin G Q. *Advanced Materials Research*[J], 2012, 578: 202
- 20 Luan B F, Qiu R S, Zhou Z et al. *International Conference on Nuclear Engineering*[C]. New York: ASME International, 2013
- 21 Sarkar A, Chakravarty J K. *Journal of Nuclear Materials*[J], 2013, 440(1-3): 136
- 22 Saxena K K, Pancholi V, Chaudhari G P et al. *Materials Science Forum Vol. 890*[C], Bäch: Trans Tech Publications Ltd, 2017: 319
- 23 Chakravarty J K, Kapoor R, Banerjee S et al. *Journal of Nuclear Materials*[J], 2007, 362(1): 75
- 24 Sarkar A, Chandanshive S A, Thota M K et al. *Journal of Alloys and Compounds*[J], 2017, 703: 56
- 25 Saxena K K, Suresh K S, Kulkarni R V et al. *Journal of Alloys and Compounds*[J], 2018, 741: 281
- 26 Saxena K K, Pancholi V. *Metals and Materials International*[J], 2021, 27: 2106
- 27 Sarkar A, Kapoor R, Verma A et al. *Journal of Nuclear Materials*[J], 2012, 422(1-3): 1
- 28 Chakravarty J K, Dey G K, Banerjee S. *Journal of Nuclear Materials*[J], 1995, 218(2): 247
- 29 Feng Z H, Jiang X J, Zhou Y K et al. *Progress in Natural Science: Materials International*[J], 2015, 25(5): 496
- 30 Sellars C M, McTegart W J. *Acta Metallurgica*[J], 1966, 14(9): 1136
- 31 Prasad Y V R K, Gegel H L, Doraivelu S M et al. *Metallurgical Transactions A*[J], 1984, 15: 1883
- 32 Prasad Y V R K, Seshacharyulu T. *Materials Science and Engineering A*[J], 1998, 243(1-2): 82

## Zr-Sn-Nb-Fe-Cr 合金热变形行为及加工图

李宇力, 李 豪, 陈秋羽, 周 宣, 马天洋, 孙涛涛

(西安西部新锆科技股份有限公司, 陕西 西安 710016)

**摘 要:** 通过 Gleeble3800 单轴热压缩实验, 研究了感应淬火态 Zr-Sn-Nb-Fe-Cr 合金锻棒在 600–900 °C 温度范围内和应变速率为 0.001–1 s<sup>-1</sup> 范围内的热变形特性。结果表明: 在感应淬火态 Zr-Sn-Nb-Fe-Cr 合金锻棒的真应力-真应变曲线中, 流变应力随应变速率的降低和变形温度的升高而减小。且该材料的热变形特性可以采用双曲正弦本构方程来描述, 在本实验条件下, 该合金的平均热激活能  $Q=412.9105$  kJ/mol。热加工图和热压缩后样品的微观组织分析表明, 在 600–900 °C 的温度范围和 0.001–1 s<sup>-1</sup> 的应变速率范围内, 该合金的最佳热加工参数为 795–900 °C, 0.001–0.0068 s<sup>-1</sup>。

**关键词:** 锆合金; 本构方程; 热变形; 热加工图

**作者简介:** 李宇力, 男, 1987 年生, 博士, 高级工程师, 西安西部新锆科技股份有限公司, 陕西 西安 710016, E-mail: 15503511186@163.com